

Electrical anisotropy in high-Tc granular superconductors in a magnetic field

*Original*

Electrical anisotropy in high-Tc granular superconductors in a magnetic field / Daghero, Dario; Mazzetti, Piero; Stepanescu, Aurelia; Tura, P.; Masoero, A. .. - In: PHYSICAL REVIEW. B, CONDENSED MATTER AND MATERIALS PHYSICS. - ISSN 1098-0121. - STAMPA. - 66:18(2002), pp. 184514-1-184514-10. [10.1103/PhysRevB.66.184514]

*Availability:*

This version is available at: 11583/1403497 since:

*Publisher:*

APS The Americal Physical Society

*Published*

DOI:10.1103/PhysRevB.66.184514

*Terms of use:*

This article is made available under terms and conditions as specified in the corresponding bibliographic description in the repository

*Publisher copyright*

(Article begins on next page)

**Electrical anisotropy in high- $T_c$  granular superconductors in a magnetic field**

D. Daghero, P. Mazzetti,\* A. Stepanescu, and P. Tura

*INFM–Dipartimento di Fisica, Politecnico di Torino, C.so Duca degli Abruzzi, 24-10129 Torino, Italy*

A. Masoero

*INFM–Dipartimento di Scienze e Tecnologie Avanzate dell’Università, del Piemonte Orientale “Amedeo Avogadro,” Corso Borsalino, 54-10131 Alessandria, Italy*

(Received 19 March 2002; revised manuscript received 9 August 2002; published 26 November 2002)

We propose an analytical model devoted to explain the anisotropy of the electrical resistance observed below the critical temperature in granular high- $T_c$  superconductors submitted to a magnetic field  $\mathbf{H}$ . Reported experimental results obtained on a YBCO sample show that the superconducting transition occurs in two stages, with a steep drop of the resistance at  $T_c$  and a subsequent, smoother decrease. In this second stage, the resistance versus temperature curve is strongly dependent not only on the field intensity, but also on the angle between  $\mathbf{H}$  and the macroscopic current density  $\mathbf{j}$ . We start from the assumption that the resistance below  $T_c$  is mainly due to the weak links between grains. In the model, weak links are thought of as flat surface elements separating adjacent grains. We calculate the probability for a weak link to undergo the transition to the resistive state as a function of the angle it makes with the external magnetic field  $\mathbf{H}$  and the macroscopic current density  $\mathbf{j}$ . In doing this, an important role is given to the strong nonuniformity of the local magnetic field within the specimen, due to the effect of the screening supercurrents flowing on the surface of the grains. Finally, we calculate the electrical resistance of the sample in the two cases  $\mathbf{H} \perp \mathbf{j}$  and  $\mathbf{H} \parallel \mathbf{j}$ . The predictions of this simple model turn out to be in reasonable agreement with reported experimental results obtained on a YBCO granular specimen.

DOI: 10.1103/PhysRevB.66.184514

PACS number(s): 74.25.Fy, 74.50.+r

**I. INTRODUCTION**

If a granular sample of a high- $T_c$  superconductor (HTSC) is cooled down to its critical temperature (let us call it  $T_{c0}$ ) in the presence of a magnetic field, its electrical resistance suddenly falls to a value that can be as low as 30% of the normal-state resistance just above  $T_{c0}$  (see Fig. 5 in Sec. IV). This effect, common to many cuprates, is due to the superconducting transition of the grains while the intergrain regions (weak links) remain in the resistive state.<sup>1</sup> On further cooling, the sample resistance gradually decreases, eventually becoming zero at a temperature  $T_c$  whose value depends on the applied magnetic field. In this second stage of the superconducting transition, the transport properties of the specimen are entirely controlled by the weak links between grains, that can be thought of as superconductor–normal conductor–superconductor Josephson junctions<sup>2</sup> with randomly distributed critical energies. According to this approach, when the temperature is lowered the superconducting wave functions of the grains gradually lock in phase. This gives rise to long-range coherence and finally to the bulk superconductivity. Of course, the transition of each junction from the superconducting to the resistive state (or vice versa) is controlled by the temperature, the current density crossing the junction and the local magnetic field. These three parameters, together with the distribution of the Josephson critical energies, are thus expected to play a major role in determining the electrical behavior of the material. The transition also depends on whether the magnetic field is applied during the cooling of the sample [field cooling (FC)] or after cooling [zero field cooling (ZFC)]. Actually, in the FC case field penetration and trapping within the grains re-

duces the transition probability of the weak links, and consequently the value of the electrical resistance, by reducing the flux compression factor. This last quantity will be introduced and discussed in Sec. III of this paper.

Finally, in many cases, the electrical properties of granular HTSC below  $T_{c0}$  are found to depend on the angle between the magnetic field  $\mathbf{H}$  and the macroscopic current density  $\mathbf{j}$ , even if the grains are randomly oriented. This indicates the existence of an electrical anisotropy of the material, induced by the application of an external magnetic field. That also this anisotropy is related to the complex transition dynamics of the weak link network is demonstrated by its almost complete absence in high-density polycrystalline MgB<sub>2</sub> samples, where grains are connected through metallic contacts and there are no weak links.<sup>3</sup>

In the following, we will propose an explanation for the observed electrical anisotropy in a zero-field-cooled granular HTSC. The leading idea of the model is that the screening supercurrents flowing on the surface of the superconducting grains create a local “demagnetizing field” that adds to the external one creating a strongly nonuniform field distribution in the intergrain regions. We will show that this field distribution gives rise to a structural anisotropy in the network of resistive weak links, so that the material behaves as a uniaxially anisotropic medium for the current transport. By starting from simple hypotheses, which will be discussed and supported by experimental evidence, we will develop a simple network model that allows calculation of the electrical resistance of the material as a function of the magnetic field and of the current density in the two cases where  $\mathbf{H} \perp \mathbf{j}$  and  $\mathbf{H} \parallel \mathbf{j}$ . Finally, we will compare the results of our calculations with

an extensive set of experimental results obtained on a YBCO granular specimen.

## II. THE APPROACH TO THE PROBLEM

Let us focus on a zero-field-cooled granular superconductor. Suppose to feed it with a current of density  $\mathbf{j}$  and to apply a magnetic field  $\mathbf{H}$  such that the bulk superconductivity is disrupted, but the grains remain in the Meissner state. As long as the grains exclude the magnetic field, experiments show that the resistance versus magnetic field curves are very nearly reversible. This reversibility shows that it is the flux pinning within the grains that originates the hysteresis, while flux pinning in the intergrain regions is negligible. In these conditions, the electrical resistance is found to depend on whether the magnetic field  $\mathbf{H}$  and the macroscopic current density  $\mathbf{j}$  are parallel or perpendicular to each other. This anisotropy was already seen by some measurements of critical current,<sup>4,5</sup> resistivity,<sup>6,7</sup> magnetization,<sup>8</sup> power dissipation,<sup>9</sup> and  $I$ - $V$  characteristics<sup>10</sup> in different HTSC's. Most of the relevant papers propose an explanation for the anisotropy based on the conventional theories of the current-driven vortex motion in the mixed state. Within this picture, the anisotropy arises from the fact that the Lorentz force between transport current and vortices depends on the angle between  $\mathbf{H}$  and  $\mathbf{j}$ . Actually, this requires that the material behaves as a nearly homogeneous medium with an effective penetration depth  $\lambda_{\text{eff}}$ , where the magnetic flux penetrates in the form of vortices as in conventional type-II superconductors. As pointed out by Ginzburg *et al.*<sup>11</sup> this approach is reasonable as long as  $\lambda_{\text{eff}}$  is much greater than the average grain size, and fluxons can be taken parallel to the external field. Even in this case, however, the conventional theories must be improved—for example, to explain why, in the  $\mathbf{H}\parallel\mathbf{j}$  case, the voltage drop across the specimen is far from being nearly zero. Finally, experimental results that will be presented in the following section clearly indicate that the anisotropy gradually vanishes when the temperature approaches  $T_{c0}$ , and this behavior is not easily explicable within the picture described so far.

In the following we will propose a completely different explanation for the electrical anisotropy induced in granular HTSC's by the magnetic field. We will start by representing the material as a set of irregularly shaped grains connected through thin intergrain regions that behave as weak links. We will think of these weak links as resistively shunted Josephson junctions with a perfect Ohmic behavior in the normal state—that is, with a normal-state resistance independent of both magnetic field and current, as well as of the angle between them. This assumption again finds support in the fact that, at temperatures close to  $T_{c0}$ , when almost all the weak links are in the resistive state, the anisotropy disappears. This suggests that the anisotropy is related to the *spatial distribution* of superconductive and resistive weak links within the material, rather than to an intrinsic dependence of the intergrain resistivity on the orientation of  $\mathbf{H}$  and  $\mathbf{j}$ .

The problem now is to understand why the distribution of resistive weak links should be anisotropic. We argue that this distribution is mainly determined by the distribution of the

local magnetic field intensity in the intergrain region. As a matter of fact, the local magnetic field  $\mathbf{H}_l$  is given by the superposition of the external field  $\mathbf{H}$  and of the magnetic field created by the screening supercurrents that flow on the grain surfaces. As a result, the local field intensity  $H_l$  in a given weak link can be very different from  $H$ , and can vary very drastically from one weak link to another. Simple geometrical considerations lead to the conclusion that this variation is related to the spatial orientation of the weak links with respect to  $\mathbf{H}$ . The strong nonuniformity of the local field makes the transition probability of the weak links anisotropic. Therefore, the spatial distribution of weak links that undergo the transition to the resistive state becomes anisotropic as well, and the material behaves as a uniaxially anisotropic medium for the current.

The influence of the screening supercurrents of the grains on the intergrain region was already invoked to explain other interesting properties of granular superconductors, such as the hysteresis of the critical current<sup>12–15</sup> and the ac magnetization curves.<sup>8</sup> In the original approach by Evetts and Glowacki<sup>12</sup> it was assumed that a sufficiently weak magnetic field can be excluded both by grains and by superconducting “islands” bounded by closed paths, called “rings,” made up of grains connected through weak links with relatively high critical currents. According to their discussion, the screening supercurrents flowing along the boundaries of the superconducting regions create “flux compression” in the surrounding weak links where the field has penetrated, which thus experience a magnetic field more intense than the applied one. It is worthwhile to notice that, in that paper, the local magnetic field outside the superconducting regions was supposed to be *everywhere* greater than the applied field.

In contrast, experimental studies of the ac magnetization of granular HTSC's led Chandran and Chaddah<sup>8</sup> to suggest that the screening supercurrents flowing on the grain surface give rise to flux compression in the weak links laying on planes parallel to the external field  $\mathbf{H}$ , and to an almost complete magnetic shielding of the weak links perpendicular to  $\mathbf{H}$ . In spite of the oversimplification implicit in this model—grains are thought to be cubic and arranged in a regular lattice, as in Fig. 1—the idea it is based on can be safely assumed to explain the origin of the magnetic field-induced anisotropy of the resistance in granular superconductors.

In the present paper, we shall neglect the possible contribution of superconducting “rings” to the non-uniformity of the local magnetic field in the intergrain regions. Actually, the experimental results to which we will compare the theoretical predictions of our model were obtained on a YBCO granular specimen with a small critical current density (less than  $10^5$  A/m<sup>2</sup> at  $T=27$  K). A simple calculation shows that the maximum magnetic field created by this current density flowing on a circular ring made up of grains and superconducting weak links is definitely negligible with respect to the magnetic fields considered here, even if the ring is very small. Notice that also in Refs. 14 and 15 experimental results were reported, suggesting that flux trapping or exclusion is mostly due to the grains, rather than to persistent superconducting loops in the weak link network.

The model we are going to present in the following arises

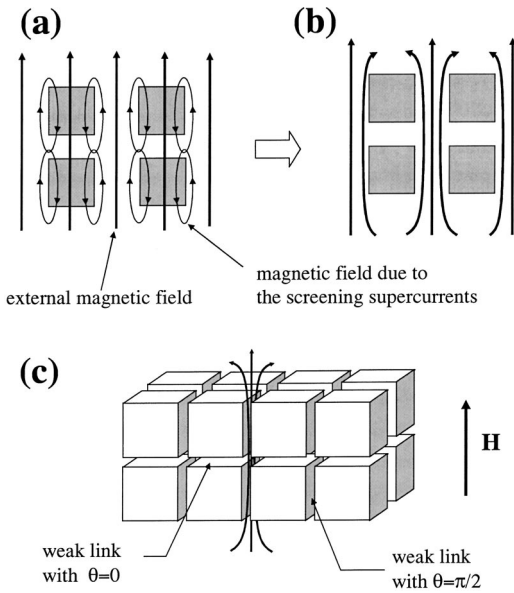


FIG. 1. In the simplest model for a polycrystalline HTSC, grains are cubic, arranged in a regular lattice and separated from each other by intergrain regions that behave as weak links. (a) If a weak magnetic field (thick arrows) is applied to the zero-field-cooled material, the screening supercurrent flowing on the surface of each grain creates a demagnetizing field (thin loops with arrows). (b) The effective field in the intergrain region results from the superposition of the demagnetizing fields of different grains and of the applied magnetic field. (c) The resulting field pattern is such that the magnetic field is zero in the weak links with  $\theta=0$ , and is greater than the applied one in the weak links with  $\theta=\pi/2$ . This field enhancement is usually referred to as “flux compression.”

from a generalization of the idea by Chandran and Chaddah<sup>8</sup> to a more realistic case, in which the grains have irregular shape and the weak links are randomly oriented in space. We will show that this model quantitatively explains the results of a set of resistance measurements we carried out on a YBCO granular specimen.

### III. THE MODEL

#### A. The simplest case

To discuss the origin of the field-induced resistance anisotropy in granular HTSC's, let us start with the analysis of the ideal, simplified case in which the material is made up of a set of identical cubic grains arranged in a regular lattice, as shown in Fig. 1. Within this simple picture, the weak links are represented by the flat, square surfaces separating adjacent grains. Let the magnetic field  $\mathbf{H}$  be applied parallel to one of the grain edges, for example along the vertical direction. As previously discussed,  $\mathbf{H}$  is assumed to be intense enough to destroy the magnetic screening of the sample as a whole (due to the supercurrent flowing on the sample surface), but weak enough not to penetrate into the grains. Let  $\theta$  be the angle between the field  $\mathbf{H}$  and the normal  $\mathbf{n}$  to a given weak-link surface. It is clear that, in this simple model, only the values  $\theta=0$  (corresponding to  $\mathbf{n}\parallel\mathbf{H}$ ) and  $\theta=\pi/2$  (corresponding to  $\mathbf{n}\perp\mathbf{H}$ ) are possible.

The screening supercurrents flowing on the surface of each grain, which is supposed to be in the Meissner state, create a “demagnetizing field” that cancels out the external magnetic field  $\mathbf{H}$  inside the grain. In the surrounding weak links, the local magnetic field  $\mathbf{H}_l$  is given by the superposition of the demagnetizing fields of adjacent grains and of the external field  $\mathbf{H}$ . As shown in Fig. 1, the resulting local magnetic field is much more intense than the external one (i.e., the flux is “compressed”) in the weak links having  $\theta = \pi/2$ , while it is zero in the weak links having  $\theta=0$ .

In the hypothesis that the weak links behave as Josephson junctions, their transition to the resistive state occurs when the density of the current crossing the junction is greater than a critical value  $j_c(T,H)$ , which depends on the temperature and on the local magnetic field. Therefore, when the current density  $\mathbf{j}$  is perpendicular to the external field  $\mathbf{H}$ , the condition for the resistive transition is easily satisfied in the weak links having  $\theta=\pi/2$ , which are crossed by the current and submitted to a strong magnetic field. The resistance of the sample is thus different from zero.

In contrast, when  $\mathbf{j}$  is parallel to  $\mathbf{H}$  the weak links having  $\theta=0$  remain in the superconducting state even though they are crossed by the current (provided that the current density is not too large) because of the magnetic screening of the grains. Therefore, each vertical column of interconnected grains behaves as a superconducting path for the current, and the specimen resistance drops to zero.

To summarize, the nonuniformity of the local magnetic field makes the spatial distribution of resistive weak links depend on the direction of  $\mathbf{j}$  with respect to  $\mathbf{H}$ . The macroscopic result is a field-induced anisotropy of the transport properties of the material (in particular, of the resistivity).

After this simple explanation of the basic mechanism, the generalization of the model to a more realistic situation, in which grains have irregular shape and size, has now to be considered. We shall adopt a statistical point of view and make some simple assumptions, consistent with the experimental conditions.

#### B. The hypotheses

Let us identify the weak links with flat elements approximating the surface separating adjacent grains, with random orientation in space and average area  $\Delta s$ . Let  $\mathbf{n}$  be the unit-length vector normal to their surface,  $\theta$  the angle between  $\mathbf{n}$  and the applied magnetic field  $\mathbf{H}$ , and  $\beta$  the angle between  $\mathbf{n}$  and the *macroscopic* current density  $\mathbf{j}$ . (Here and in the following we shall use  $\mathbf{j}$  to indicate the vectorial average of the current density within the whole specimen. Instead, the local current density will be indicated by  $\mathbf{j}_l$ .) Let  $\mathbf{H}_l$  and  $\mathbf{j}_l$  be the *local* magnetic field and current density within a weak link. Notice that, as long as the grains are in the Meissner state,  $\mathbf{H}_l$  must be *parallel* to the weak-link surface—that is, tangent to the grain boundary. We will further assume that the weak links behave as ideal resistively shunted Josephson junctions, with a perfect Ohmic behavior above the transition and that they have all the same resistive-state conductance per unit surface,  $g$ .

In principle, each weak link undergoes the transition from the superconducting to the resistive state when the local cur-

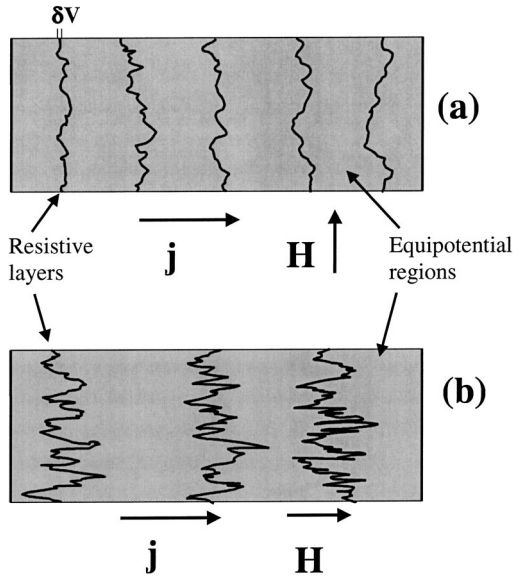


FIG. 2. Longitudinal cross section of a zero-field-cooled cylindrical polycrystalline HTSC some time after the application of a magnetic field  $\mathbf{H}$  intense enough to make it macroscopically resistive. At the equilibrium, the sample consists of equipotential superconducting regions (gray), separated by resistive layers (irregular solid lines) made up of resistive weak links. The effect of the relative orientation of  $\mathbf{H}$  and  $\mathbf{j}$  is made clear by comparing (a) with (b). It is related to the fact that the probability for a weak link to undergo the transition to the resistive state is larger when  $\mathbf{H}$  is parallel to its surface, and smaller when  $\mathbf{H}$  is perpendicular to it.

rent density  $j_l$  is greater than a critical value  $j_{l,c}(H_l, T)$ . However, complex transient phenomena occurring at the beginning of the conduction process make it very difficult to determine the actual spatial distribution of the resistive weak links. These phenomena are due to correlation effects acting on the local current distribution, which, for instance, prevent the weak links embedded in a superconducting region to undergo the resistive transition. Anyway, when the whole specimen becomes macroscopically resistive, a stationary situation similar to that sketched in Fig. 2 must be reached. At equilibrium, the specimen must be thought of as divided into a set of equipotential regions separated by resistive layers extended throughout the specimen cross section.

The equipotential regions consist of several superconducting grains and of the weak links between them. Of course, all these weak links must be in the superconducting state, since any potential drop within these regions is forbidden. It is worthwhile to notice that the magnetic flux *may* penetrate within the weak links embedded in an equipotential region, but the local current density should remain below its critical value to avoid the resistive transition.

The resistive layers, instead, are made up of resistive weak links. Since these layers separate two regions at different potential, the local current density  $\mathbf{j}_l$  that crosses them must be always *perpendicular* to their surface, while the local magnetic field  $\mathbf{H}_l$  is tangent to it. Since the weak links are assumed to behave as ideal shunted Josephson junctions with perfect Ohmic behaviors above the transition, the electrical resistance of each layer may be considered as independent of

both  $\mathbf{H}_l$  and  $\mathbf{j}_l$ . As already pointed out, this last assumption is supported by the resistance versus temperature curves reported in Fig. 5, measured in a YBCO granular specimen described in Sec. IV.

At a given temperature, the transition of a weak link to the resistive state is completely determined by  $\mathbf{H}_l$  and  $\mathbf{j}_l$ . As a good approximation, we can say that the transition occurs when

$$j_l = j_{l,0}(T) \frac{H_0}{\pi H_l}, \quad (1)$$

where  $j_{l,0}(T)$  is the value of the local critical current density in zero magnetic field, and  $H_0$  is given by

$$H_0 = \frac{\phi_0}{4\mu_0\lambda(T)R_g}.$$

Here  $\lambda(T)$  is the magnetic penetration depth,  $R_g$  is the mean radius of the grains, and  $\phi_0$  is the flux quantum. Equation (1) represents the envelope of the Fraunhofer-like  $I$  vs  $H$  curve of a single Josephson junction in the presence of a magnetic field parallel to the junction itself.<sup>2</sup> Using the envelope instead of the true function is usual when a statistical approach is needed, i.e., when a large number of junctions enter into the model. Actually, as far as the inverse proportionality between  $j_l$  and  $H_l$  is concerned, the validity of Eq. (1) is supported by experimental results that will be discussed in Sec. IV.

For any given value  $j_l$  of the current density, Eq. (1) can be interpreted as a condition on the intensity of the local magnetic field  $H_l$ . The critical value of  $H_l$  giving rise to the transition will be indicated in the following by

$$H_c(j_l) = H_0 \frac{j_{l,0}(T)}{\pi j_l}. \quad (2)$$

With reference to the equilibrium situation described in Fig. 2, the local current density in a resistive weak link is given by

$$j_l = \mathbf{j} \cdot \mathbf{n} = j \cos \beta.$$

Thus, Eq. (2) becomes

$$H_c(j_l) = H_0 \frac{j_{l,0}(T)}{\pi j} \frac{1}{\cos \beta} = H_c(j) \frac{1}{\cos \beta}. \quad (3)$$

We will assume that, for a given value of the local current density, the critical fields  $H_c(j_l)$  of the weak links follow a Gaussian distribution with mean value  $\langle H_c(j_l) \rangle$  and standard deviation  $\sigma_c$ . In fact, the fluctuation of  $H_c(j_l)$  around its mean value—within the weak-link ensemble characterized by a given value of  $\mathbf{j}_l$ —is due to several uncorrelated causes: the grain orientation mismatch, impurity segregation at the grain boundaries, nonstoichiometric local oxygen content, etc. In these cases the assumption that the fluctuation is Gaussian is generally accepted. We further assume that  $\sigma_c$  is proportional to  $\langle H_c(j_l) \rangle$ . This assumption can be justified by observing that when  $\langle H_c(j_l) \rangle$  is, for instance, reduced as a consequence of an increment of  $j_l$ , also the fluctuation

around its value must change accordingly. Actually, it must be noticed that  $\langle H_c(j_l) \rangle$  depends on  $j_l$  and thus on the spherical angles  $\theta$  and  $\varphi$ , and that the average is intended to be made over the set of weak links characterized by given values of these angles.

Equation (3) indicates that the critical field of each weak link depends on the angle  $\beta$  between its normal  $\mathbf{n}$  and the current density  $\mathbf{j}$ . However, the intensity of the local magnetic field in the weak link,  $H_l$ , is expected to depend in some way on the angle  $\theta$  between  $\mathbf{n}$  and  $\mathbf{H}$ . That this dependence should exist is suggested by the simple model of cubic grains, where the value of the local field was easily determined for all the allowed values of  $\theta$ . In the more realistic case of irregular-shaped grains we are facing here, flux lines meander through the sample, without violating the requirement of continuity. It is thus very likely, for instance, that flux lines are forced to pass through weak links with a very low value of  $\theta$ , or that weak links with  $\theta$  close to  $\pi/2$  are almost completely screened. Since the value of  $H_l$  in a given weak link characterized by an angle  $\theta$  also depends on the position and on the angle distribution of the nearby weak links, it is reasonable to assume also in this case a Gaussian distribution of  $H_l(\theta)$  around its mean value  $\langle H_l(\theta) \rangle$  with a variance  $\sigma_l$  proportional, as in the previous case, to  $\langle H_l(\theta) \rangle$ . Since  $\mathbf{H}_l$  should always be tangent to the grain surface, we can rather safely assume that the dependence of  $\langle H_l(\theta) \rangle$  on  $\theta$  is expressed by the equation:

$$\langle H_l(\theta) \rangle = H' \sin \theta \quad (4)$$

analogous to the expression of the local magnetic field intensity on the surface of a superconducting sphere immersed in a uniform magnetic field.<sup>16</sup> In this equation,  $H'$  is a constant magnetic field intensity that is related to the external magnetic field through a ‘‘flux compression factor’’  $k$  that takes into account the effect of the flux exclusion by the grains. Finding an explicit expression for  $k$  will be the aim of the following section.

### C. Flux compression factor $k$

Let us now assume that the magnetic field  $\mathbf{H}$  is applied parallel to the  $z$  axis (whose direction is defined by the unit-length vector  $\mathbf{u}_z$ ). To determine the value of  $H'$ , we first write down an expression for the mean value of the  $z$  component of  $\mathbf{H}_l$  over the ensemble of weak links with the same  $\theta$ . With reference to Fig. 3 one finds

$$\langle H_{l,z}(\theta) \rangle = \langle H_l(\theta) \sin \theta \rangle = \langle H_l(\theta) \rangle \sin \theta = H' (\sin \theta)^2. \quad (5)$$

The mean value of the  $z$  component over all the weak link ensemble is now given by a simple solid angle average:

$$\langle H_{l,z} \rangle = \langle \langle H_{l,z}(\theta) \rangle \rangle_\theta = \frac{1}{4\pi} \int H' (\sin \theta)^2 d\Omega = \frac{2}{3} H'. \quad (6)$$

In order to find the compression factor, we express the same quantity in a different way. In fact, if no superconducting rings survive, the magnetic field is only excluded by the grains and its dispersion at the sample edges is expected to

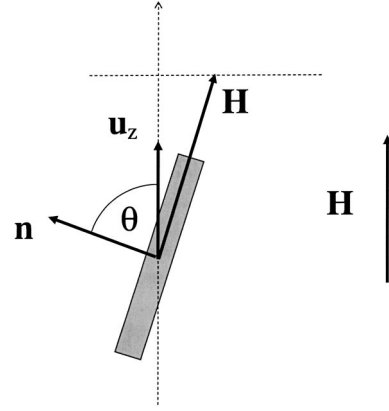


FIG. 3. Representation of the vectors characterizing the position of a single weak link. The figure also shows that the local magnetic field is always parallel to the weak-link surface.  $\theta$  is the angle between the unit-length vector normal to the surface,  $\mathbf{n}$ , and the applied magnetic field  $\mathbf{H}$ .

be negligible. In these conditions, the magnetic flux  $\Phi$  is very nearly constant all along the specimen and obviously equal to  $HA_H$ , where  $H$  is the intensity of the applied magnetic field  $\mathbf{H}$  (which is taken parallel to the  $z$  axis) and  $A_H$  is the specimen cross section perpendicular to it. On the other hand, the explicit calculation of the flux gives

$$\Phi = \int_{A_H} \mathbf{H}_l \cdot \mathbf{u}_z dS = \int_{A_H} H_{l,z} dS = \langle H_{l,z} \rangle A_H'. \quad (7)$$

The integral has been restricted to the portion  $A_H'$  of the specimen cross section in which the magnetic field has penetrated. Provided that there is no flux penetration into the grains,  $A_H'$  can be taken as a constant quantity. Finally,  $\langle H_{l,z} \rangle$  is obviously the mean value of  $H_{l,z}$  over  $A_H'$ .

Comparing Eq. (7) with the equality  $\Phi = HA_H$  gives

$$\langle H_{l,z} \rangle = H \frac{A_H}{A_H'} \quad (8)$$

and, by comparing this result with Eq. (6), an expression for  $H'$  is finally obtained:

$$H' = \frac{3}{2} \frac{A_H}{A_H'} H = kH, \quad k = \frac{3}{2} \frac{A_H}{A_H'}. \quad (9)$$

In conclusion, taking into account Eq. (4), the mean value of the local field intensity obtained by averaging over all the weak links with the same  $\theta$  can be written:

$$\langle H_l(\theta) \rangle = kH \sin \theta. \quad (10)$$

### D. Transition probability for the weak links

As previously pointed out, we suppose that a weak link with a given value of  $\theta$  undergoes the transition to the resistive state when the local magnetic field within it,  $H_l(\theta)$ , becomes equal to a current-dependent critical field  $H_c(j_l)$ . The transition probability for this weak link is thus:

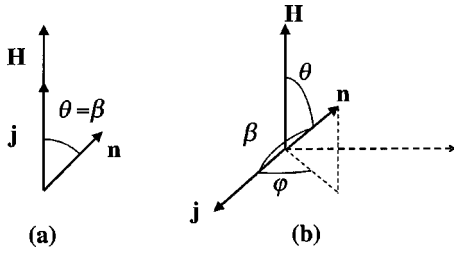


FIG. 4. Graphic representation of the vectors  $\mathbf{H}$ ,  $\mathbf{j}$ , and  $\mathbf{n}$  in the two cases where (a)  $\mathbf{H}\parallel\mathbf{j}$  and (b)  $\mathbf{H}\perp\mathbf{j}$ .

$$P^{\text{tr}}(\theta, \beta) = \int_{-\infty}^{+\infty} f(H_l|\theta) P(H_l \geq H_c(j_l)) dH_l, \quad (11)$$

where  $f(H_l|\theta)$  is the distribution of the local field intensity for a given  $\theta$ , and  $P(H_l \geq H_c(j_l))$  is the probability for  $H_l$  to be greater than  $H_c(j_l)$ . According to previous assumptions,  $f(H_l|\theta)$  can be written

$$f(H_l|\theta) = \frac{1}{\sqrt{2\pi}\sigma_l} \exp\left[-\frac{(H_l - kH \sin \theta)^2}{2\sigma_l^2}\right], \quad (12)$$

where Eq. (10) has been used to express the mean value of  $H_l(\theta)$ . Similarly, the expression for  $P(H_l \geq H_c(j_l))$  reads:

$$\begin{aligned} P(H_l \geq H_c(j_l)) &= \int_0^{H_l} \frac{1}{\sqrt{2\pi}\sigma_c} e^{-[H_c - \langle H_c(j) \rangle]^2 / 2\sigma_c^2} dH_c \\ &= \frac{1}{2} \left[ 1 + \operatorname{erf}\left(\frac{H_l - \langle H_c(j) \rangle / \cos \beta}{\sqrt{2}\sigma_c}\right) \right], \end{aligned} \quad (13)$$

where Eq. (3) has been used to express  $\langle H_c(j) \rangle$  in terms of the angle  $\beta$ . It can be noticed that Eq. (11) already contains all the information about the field-induced anisotropy we are dealing with in the present paper, in the sense that  $P^{\text{tr}}$  will have a different expression as the current density  $\mathbf{j}$  is parallel or perpendicular to the applied magnetic field  $\mathbf{H}$ . As a matter of fact, the relationship between  $\beta$  and  $\theta$  is different in the two cases. With reference to Fig. 4, it is clear that

$$\cos \beta = \cos \theta \quad \text{if } \mathbf{H}\parallel\mathbf{j} \quad (14)$$

$$\cos \beta = \sin \theta \cos \varphi \quad \text{if } \mathbf{H}\perp\mathbf{j}, \quad (15)$$

where  $\varphi$  is the angle between  $\mathbf{j}$  and the plane containing both  $\mathbf{H}$  and  $\mathbf{n}$ . Taking into account Eqs. (14) and (15), we shall indicate the transition probability functions for  $\mathbf{H}\parallel\mathbf{j}$  and  $\mathbf{H}\perp\mathbf{j}$  as  $P_{\parallel}^{\text{tr}}(\theta)$  and  $P_{\perp}^{\text{tr}}(\theta, \varphi)$ , respectively. By using Eqs. (11)–(13), and by taking into account the expressions for  $\cos \beta$  given in Eqs. (14) and (15), one obtains

$$\begin{aligned} P_{\parallel}^{\text{tr}}(\theta) &= \int_{-\infty}^{+\infty} \frac{1}{\sqrt{2\pi}\sigma_l} \exp\left[-\frac{(H_l - kH \sin \theta)^2}{2\sigma_l^2}\right] \\ &\quad \times \frac{1}{2} \left[ 1 + \operatorname{erf}\left(\frac{H_l - \langle H_c(j) \rangle / \cos \theta}{\sqrt{2}\sigma_c}\right) \right] dH_l \end{aligned} \quad (16)$$

and

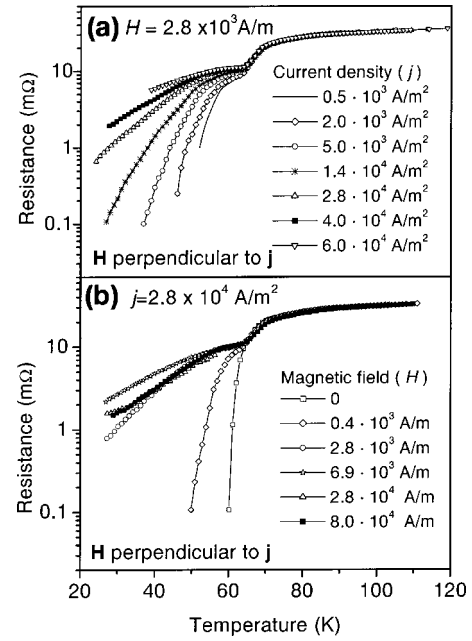


FIG. 5. Experimental  $R$ -vs- $T$  curves measured in the YBCO specimen described in the paper, in the presence of a magnetic field  $\mathbf{H}$  perpendicular to the current density  $\mathbf{j}$ . The curves in (a) were measured with a magnetic field of intensity  $H = 2.8 \times 10^3$  A/m and different values of the current density. The curves in (b), instead, were obtained with a current density  $j = 2.8 \times 10^4$  A/m<sup>2</sup> and different values of the applied magnetic field. The drop of the resistance at the temperature  $T_{c0} \approx 65$  K is due to the superconducting transition of the grains, while the intergrain regions remain in the resistive state. Notice that the residual resistance just below  $T_{c0}$  (that is, the resistance of the whole weak-link network) is almost independent of both the current density and the magnetic field.

$$\begin{aligned} P_{\perp}^{\text{tr}}(\theta, \varphi) &= \int_{-\infty}^{+\infty} \frac{1}{\sqrt{2\pi}\sigma_l} \exp\left[-\frac{(H_l - kH \sin \theta)^2}{2\sigma_l^2}\right] \\ &\quad \times \frac{1}{2} \left[ 1 + \operatorname{erf}\left(\frac{H_l - \langle H_c(j) \rangle / \sin \theta \cos \varphi}{\sqrt{2}\sigma_c}\right) \right] dH_l. \end{aligned} \quad (17)$$

### E. Calculation of the specimen resistance

As discussed above, when the specimen resistance is different from zero, the specimen itself can be described as a series of equipotential stripes, separated by thin layers made of resistive weak links. The dependence of the transition probability of the weak links on their angular position makes these resistive layers look very different in the two cases  $\mathbf{H}\parallel\mathbf{j}$  and  $\mathbf{H}\perp\mathbf{j}$ , as shown in Fig. 2. Since, in agreement with the experimental results reported in Fig. 5, all the weak links are assumed to have the same resistive-state conductance per unit surface  $g$ , the conductance of each layer is simply proportional to its area  $S$ . The mean value of the area  $S$  can be easily calculated by taking into account that each layer is made of *resistive* weak links, and that its projection on a plane perpendicular to the current density  $\mathbf{j}$  must be equal to the specimen cross-section area  $A_j$ :

$$\langle S \rangle = \frac{A_j}{\langle |\cos \beta| \rangle_{\text{res}}}. \quad (18)$$

Here, the subscript res means that the average is made over the ensemble of the resistive weak links. Thus

$$\langle |\cos \beta| \rangle_{\text{res}} = \frac{\int P^{\text{tr}}(\theta, \beta) |\cos \beta| d\Omega}{\int P^{\text{tr}}(\theta, \beta) d\Omega}, \quad (19)$$

where  $P^{\text{tr}}$  is given by Eq. (16) or Eq. (17) according to whether  $\mathbf{H} \parallel \mathbf{j}$  or  $\mathbf{H} \perp \mathbf{j}$ , and the integrals are extended to the whole solid angle  $\Omega = 4\pi$ . The mean value of the resistance of each layer is thus

$$r = \frac{1}{\langle S \rangle g} = \frac{\langle |\cos \beta| \rangle_{\text{res}}}{g A_j}. \quad (20)$$

Let  $n_L$  be the number of resistive layers: the resistance of the specimen is thus given by

$$R = n_L r = n_L \frac{\langle |\cos \beta| \rangle_{\text{res}}}{g A_j}. \quad (21)$$

To evaluate  $n_L$ , we must first calculate the total number of resistive weak links,  $N$ , involved in the creation of a given pattern of resistive layers.  $N$  is proportional to the integral of the transition probability of the weak links,  $P^{\text{tr}}$ , over the whole space. More precisely, if  $N_T$  is the total number of weak links in the whole specimen,  $N$  is given by

$$N = N_T \int P^{\text{tr}}(\theta, \beta) d\Omega. \quad (22)$$

On the other hand, the number of weak links that compose a *single* resistive layer,  $n_w$ , is

$$n_w = \frac{\langle S \rangle}{\Delta s} = \frac{A_j}{\Delta s \langle |\cos \beta| \rangle_{\text{res}}}, \quad (23)$$

where  $\Delta s$  is the average area of a resistive weak link and is of the order of the square of the grain radius  $R_g$ . Thus the number of layers is thus

$$n_L = \frac{N}{n_w} = N \frac{\Delta s \langle |\cos \beta| \rangle_{\text{res}}}{A_j}, \quad (24)$$

and the specimen resistance becomes

$$R = N \frac{\Delta s (\langle |\cos \beta| \rangle_{\text{res}})^2}{g A_j^2}. \quad (25)$$

It is worthwhile to notice that, in Eq. (25), the specimen resistance turns out to be proportional to the total number of resistive weak links. Actually, as is well known from the percolation theories applied to the superconducting transition,<sup>17</sup> this is not true in the proximity of the percolative threshold, since below a minimum number of resistive weak links not a single resistive layer is generated. This implies that below a given value of  $H$  the specimen is in the

superconducting state and obviously Eq. (25) is not valid. This point will be taken into account in comparing the theoretical results with experimental data.

### F. Anisotropy of the resistivity

As previously pointed out, all the information about the anisotropy of the resistance is already contained in the transition probability [see Eqs. (16) and (17)].  $P^{\text{tr}}$  enters directly into the calculation of the specimen resistance through the mean value of  $|\cos \beta|$  over the ensemble of resistive weak links. We shall use  $R_{\parallel}$  and  $R_{\perp}$  to indicate the resistance in the case where  $\mathbf{H} \parallel \mathbf{j}$  and  $\mathbf{H} \perp \mathbf{j}$ , respectively. According to Eqs. (25), (22), and (19), and by using the expressions for  $\cos \beta$  reported in Eqs. (14) and (15), one finds

$$R_{\parallel} = \frac{\Delta s}{g A_j^2} N_T \int P_{\parallel}^{\text{tr}}(\theta) d\Omega \left[ \frac{\int P_{\parallel}^{\text{tr}}(\theta) |\cos \theta| d\Omega}{\int P_{\parallel}^{\text{tr}}(\theta) d\Omega} \right]^2 \quad (26)$$

and

$$R_{\perp} = \frac{\Delta s}{g A_j^2} N_T \int P_{\perp}^{\text{tr}}(\theta, \varphi) d\Omega \times \left[ \frac{\int P_{\perp}^{\text{tr}}(\theta, \varphi) |\sin \theta \cos \varphi| d\Omega}{\int P_{\perp}^{\text{tr}}(\theta, \varphi) d\Omega} \right]^2. \quad (27)$$

In order to evaluate the anisotropy of the resistance (that is, its dependence on the respective orientation of  $\mathbf{H}$  and  $\mathbf{j}$ ) we shall define a parameter  $\eta$  such that

$$\eta = \frac{R_{\parallel}}{R_{\perp}} = \frac{\rho_{\parallel}}{\rho_{\perp}}. \quad (28)$$

The last equality holds because the current always flows in the same direction with respect to the specimen (and the direction of the magnetic field is changed instead). On account of Eqs. (26) and (27),  $\eta$  can be written as follows:

$$\eta = \frac{\int P_{\perp}^{\text{tr}}(\theta, \varphi) d\Omega}{\int P_{\parallel}^{\text{tr}}(\theta) d\Omega} \left[ \frac{\int P_{\parallel}^{\text{tr}}(\theta) |\cos \theta| d\Omega}{\int P_{\perp}^{\text{tr}}(\theta, \varphi) |\sin \theta \cos \varphi| d\Omega} \right]^2. \quad (29)$$

As in the preceding section, the integration domain is the whole solid angle  $\Omega$ . Actually, when the explicit calculations are carried out, the symmetries of the problem allow restricting the  $\theta$  and  $\varphi$  integrals to the range  $[0, \pi/2]$ . The parameters that can be used for fitting the experimental results are all contained into the functions  $P_{\parallel}^{\text{tr}}(\theta)$  and  $P_{\perp}^{\text{tr}}(\theta, \varphi)$  appearing in the above expression. One of these parameters is  $\langle H_c(j) \rangle$ , which is the average of the critical fields over the weak-link ensemble and can be expressed in terms of the critical current intensity  $j$ , according to Eq. (3). Another parameter is the flux-compression coefficient  $k$ , which, according to Eq.

(10), simply represents a scaling factor of the applied magnetic field intensity  $H$  in the evaluation of  $\langle H_l(\theta) \rangle$ . As already stated, the standard deviations  $\sigma_c$  and  $\sigma_l$  can be taken as proportional respectively to  $\langle H_c(j_l) \rangle$  and  $\langle H_l(\theta) \rangle$ , and the proportionality constants become therefore nondimensional parameters to be used for the fit. Actually, as we will see later, the choice of their values has little influence on the theoretical curves, and thus they can be considered as non-critical parameters for the fit. As discussed in Sec. V, the most important parameter in fitting the experimental data is  $\langle H_c(j) \rangle$ , which represents the “strength” of the weak-link ensemble characteristic of the specimen under consideration. Results of the numerical calculations are reported and discussed in Sec. V.

#### IV. EXPERIMENTAL RESULTS

In this section we report the results of an extensive set of resistance measurements we carried out on a granular YBCO specimen. The sample, of about  $1 \times 1 \times 10 \text{ mm}^3$ , was obtained by sinterization of high-purity powders of  $\text{Y}_2\text{O}_3$ ,  $\text{BaCO}_3$ , and  $\text{CuO}$  in the stoichiometry ratio 1 : 2 : 3. The oxygen content of the YBCO chains was then modified by a long-time annealing (30 days) in a controlled oxygen atmosphere at  $T=720 \text{ K}$ . This process had a twofold effect on the critical parameters of the material. First, it lowered the critical temperature down to  $T_{c0}=65 \text{ K}$ ; second, it reduced the critical current, which was found to be as low as  $2.5 \times 10^5 \text{ A/m}^2$  at  $T=27 \text{ K}$  and in zero field. While the first effect can be ascribed to a change in the oxygen doping in the grains, the second is mainly due to a strong weakening of the links between grains. This made the transport properties of the material below  $T_{c0}$  be mostly controlled by the weak links in a wide range of magnetic fields.

The resistance measurements were carried out by using the conventional four-probe technique. The four contacts were obtained by Ag evaporation at the opposite ends of the sample. Both the current and voltage leads were made of thin Pt wires fixed to the Ag contact by using Ag conductive paste. To eliminate the possible unwanted contributions of thermoelectric voltages, the current-reversal technique was used. Moreover, to avoid the small Joule heating of the sample, the current was injected into the sample only during the time strictly necessary for the measurement. The magnetic field was applied either parallel or perpendicular to the current, which was always flowing along the same direction, i.e., parallel to the longest side of the sample.

The resistance versus temperature curves reported in Fig. 5 were obtained at (a) a fixed value of the magnetic field and different current densities, or (b) at a fixed current and different magnetic fields. In both cases, the magnetic field  $\mathbf{H}$  was perpendicular to the current  $\mathbf{j}$ .

The clear step of the curves at the temperature  $T_{c0} = 65 \text{ K}$  indicates that, at this temperature, the grains become superconductive while all the weak links remain in the resistive state. It is clearly seen that the residual resistance just below  $T_{c0}$  is practically independent of both the magnetic field intensity  $H$  and the current density  $j$ . If the temperature is further lowered, instead, the  $R(T)$  curves split depending

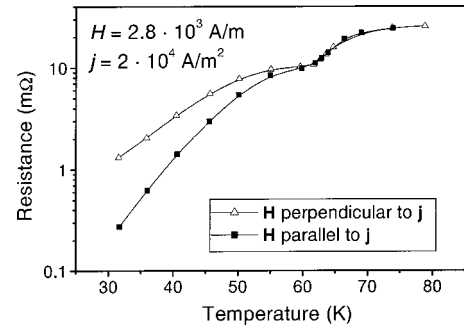


FIG. 6. Experimental  $R$ -vs- $T$  curves measured with  $j=2 \times 10^4 \text{ A/m}^2$  and  $H=2.8 \times 10^3 \text{ A/m}$ , in the two cases where  $\mathbf{H} \perp \mathbf{j}$  (open triangles) and  $\mathbf{H} \parallel \mathbf{j}$  (solid squares). Notice that the residual resistance just below  $T_{c0}$  is independent of the orientation of  $\mathbf{j}$  with respect to  $\mathbf{H}$ . As discussed in the text, this suggests that the anisotropy is not due to an intrinsic dependence of the intergrain resistivity on the angle between  $\mathbf{H}$  and  $\mathbf{j}$ .

on the values of  $H$  and  $j$ . Figure 6 shows the resistance versus temperature curves obtained with fixed values of  $H$  and  $j$  in the two cases where  $\mathbf{H} \parallel \mathbf{j}$  and  $\mathbf{H} \perp \mathbf{j}$ . It is clearly seen that the residual resistance just below  $T_{c0}$  is as well unaffected by the respective orientation of these two vectors. Since just below  $T_{c0}$  practically all the weak links are still in the resistive state, this residual resistance can be identified with that of the *whole* weak-link network. Therefore, these results indirectly support our hypothesis that the normal-state resistance of each weak link is independent of  $\mathbf{H}$  and  $\mathbf{j}$ —and thus on their respective orientation.

In order to study in greater detail the anisotropy of the resistance highlighted by the curves in Fig. 6, and to compare the predictions of our model with the experimental results, we measured the resistance of the sample as a function of the magnetic field intensity, by keeping both the temperature and the current fixed to a certain value. For example, Fig. 7 shows two sets of  $R$ -vs- $H$  curves obtained after cooling the sample down to  $T=27 \text{ K}$  in zero field, and then by applying a magnetic field  $\mathbf{H}$  perpendicular to  $\mathbf{j}$ . The two sets of curves refer to different values of the current density,  $j = 4 \times 10^4 \text{ A/m}^2$  (open and solid squares) and  $j = 6 \times 10^4 \text{ A/m}^2$  (open and solid triangles). For these values of the current density, self-field effects are very small and thus we could neglect them.

In Fig. 7, solid (open) symbols indicate the resistance measured while the magnetic field intensity is increased (decreased). It is clearly seen that the curves are very nearly reversible up to about  $4.5 \times 10^3 \text{ A/m}$ . In this regime, the magnetic flux is very likely to be excluded by the grains, and the variation of the resistance due to the magnetic field can be ascribed to the transition of weak links from the superconductive to the resistive state, or vice versa. Moreover, the curves reported in Fig. 7 show that an approximate inverse proportionality exists between the magnetic field  $H$  and the current density  $j$  for a given value of the specimen resistance. In other words, the same resistance, let us say  $R \approx 2 \text{ m}\Omega$ , is obtained with  $H \approx 1.6 \times 10^3 \text{ A/m}$  and  $j = 6 \times 10^4 \text{ A/m}^2$ , or with  $H \approx 2.4 \times 10^3 \text{ A/m}$  and  $j = 4 \times 10^4 \text{ A/m}^2$ . This is exactly

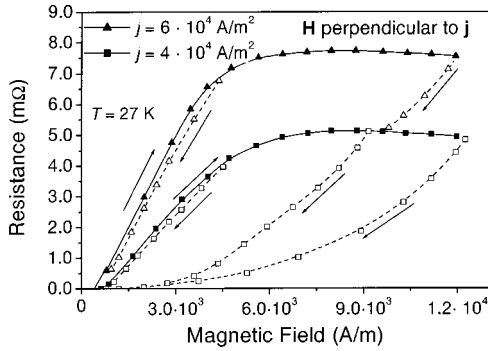


FIG. 7. Resistance versus magnetic field curves at  $T = 27$  K for two different values of the current density:  $j = 4 \times 10^4$  A/m $^2$  (squares) and  $j = 6 \times 10^4$  A/m $^2$  (triangles). The magnetic field  $\mathbf{H}$  was applied perpendicular to the current density  $\mathbf{j}$ . Solid (open) symbols indicate the resistance measured when the field is increased (decreased), as indicated by the arrows. The onset of irreversibility at  $H \approx 4.5 \times 10^3$  A/m is due to flux penetration and flux trapping inside the superconducting grains. Below this value, instead, the  $R$ -vs- $T$  curves are nearly reversible, which indicates the almost complete absence of flux trapping either by grains or by superconducting rings. In this regime, the changes in the resistance due to the magnetic field are attributed to weak-link transitions. Notice that the curves are in fair agreement with Eq. (2), since the same value of the resistance is obtained for magnetic field values inversely proportional to the current density  $j$ .

what is expected according to our model if Eq. (2) holds true and the sample is not too close to the percolation threshold.

When the field is increased above  $4.5 \times 10^3$  A/m, the magnetic flux begins to penetrate into the superconducting grains, where it remains trapped when the external field is decreased, thus giving rise to a strong hysteresis. Let us discuss for a while what happens in this irreversible regime. At the beginning of the flux penetration into the grains, the increment of the local magnetic field in the intergrain regions for a given increase of the external field is smaller than in the reversible regime. This results in a reduction of the slope of the  $R$ -vs- $H$  curve. For higher values of the applied field, the flux penetration into grains gives rise to a decrement of the local magnetic field, even if the external field is increased, and then the slope of the curve becomes slightly negative, as clearly shown in the figure. Within the model developed in the present paper, this effect can be interpreted as due to a reduction the flux compression coefficient  $k$ , which therefore turns out to depend on the magnetic field. Actually, we disregarded this dependence and took  $k$  as a constant, which is only true as long as the magnetic field *does not* penetrate into the grains. Incidentally, this is one of the reasons why the validity of our model is restricted to the reversible regime. Let us just point out here that if the field is further increased (as we did in another set of measurements not reported here) the slope becomes positive again. At about  $1.6 \times 10^5$  A/m, the resistance becomes practically constant and saturates to a current-independent value. Notice that the same behavior can be observed, close to  $T_{c0}$ , in the curves reported in Fig. 5(a).

In Fig. 8 two  $R$ -vs- $H$  curves are shown, obtained with the same values of the current density ( $4 \times 10^4$  A/m $^2$ ) but in the two cases  $\mathbf{H} \perp \mathbf{j}$  and  $\mathbf{H} \parallel \mathbf{j}$ . By starting from these data sets, the

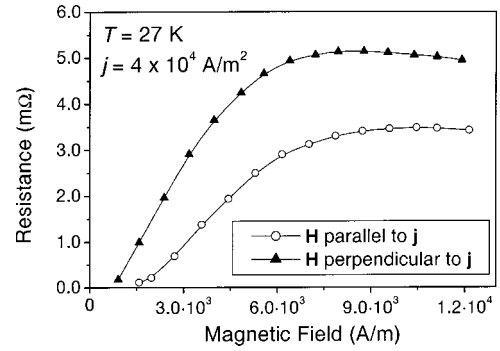


FIG. 8. Resistance vs magnetic field curves at the same values of current density and magnetic field, in the two cases where  $\mathbf{H} \perp \mathbf{j}$  (triangles) and  $\mathbf{H} \parallel \mathbf{j}$  (circles). The anisotropy of the resistance induced by the magnetic field is clearly seen. The values of  $\eta$  reported in Fig. 9 are taken from these curves and from a similar couple of curves measured with a current density  $j = 6 \times 10^4$  A/m $^2$ .

magnetic field dependence of the ratio  $\eta = R_{\parallel}/R_{\perp}$  can be easily obtained. As a matter of fact, this dependence is reported in Fig. 9 (solid triangles) together with a similar curve obtained with a current density  $j = 6 \times 10^4$  A/m $^2$  (solid squares). In the same figure, the best-fitting curves calculated by using Eq. (29) are also shown (open circles). The numerical integration of Eq. (29) was performed by means of the computer program MACSYMA version 2.2, by Macsyma, Inc. The values of the best-fit parameters, reported in the figure caption, will be discussed in the next section. Let us just point out here that, in spite of the many simplifications implicit in our model, there is fair agreement between theoretical and experimental data.

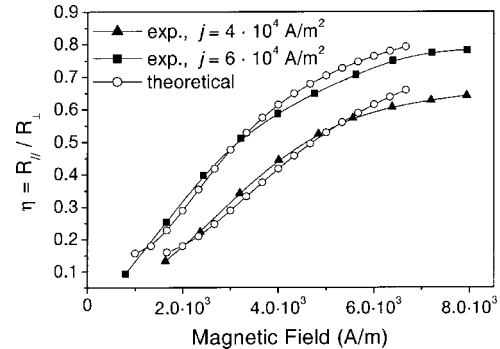


FIG. 9. Comparison between experimental and theoretical results concerning the anisotropy factor  $\eta$  for two different values of the macroscopic current density  $j$ . Solid symbols represent experimental data, while open circles represent theoretical points calculated by means of Eq. (29). The theoretical curves shown here are those that best fit the experimental data, and were obtained by taking  $H_c^*(j) = 3.0 \times 10^3$  A/m and  $H_c^*(j) = 2.0 \times 10^3$  A/m for  $j = 4 \times 10^4$  and  $6 \times 10^4$  A/m $^2$ , respectively. The ratio between the two values of  $H_c^*(j)$  clearly the inverse of the ratio between the current densities, in agreement with Eq. (2). The widths of the distributions of critical fields and local fields were taken as being  $\sigma_c = 0.3 \langle H_c(j_i) \rangle$  and  $\sigma_l = 0.7 \langle H_l(\theta) \rangle$  for both the curves. Notice that the actual values of  $\langle H_c(j_i) \rangle$  may be an order of magnitude greater than those of  $H_c^*(j)$ , owing to the effect of the flux compression coefficient  $k$ .

## V. DISCUSSION AND CONCLUSIONS

The results reported in Fig. 9 show that there is a general agreement between the experimental data and the results of our model. The agreement is particularly good for intermediate values of the magnetic field intensity. Instead, some deviations between experimental and theoretical results are evident for low and high values of the applied field. On account of what was already pointed out in the previous sections, these deviations are not surprising. As a matter of fact, our model has been developed under the assumption that the specimen was neither too close to the superconductive percolation threshold (that takes place when the magnetic field is too weak), nor in the condition of flux penetration within the grains (that occurs when the field is too intense).

Let us now focus on the best-fitting values of the parameters that enter in our model. In principle, the adjustable parameters of the model are the mean critical field  $\langle H_c(j) \rangle$ , the flux compression factor  $k$ , and the standard deviations  $\sigma_l$  and  $\sigma_c$ , characterizing the spread of the local values of  $H_l(\theta)$  and  $H_c(j)$ . Since, according to the assumptions made above,  $\sigma_l$  and  $\sigma_c$  are taken as being proportional to  $\langle H_l(\theta) \rangle$  and  $\langle H_c(j) \rangle$ , respectively, it can be easily shown that  $P_{\parallel}^{\text{tr}}(\theta)$  and  $P_{\perp}^{\text{tr}}(\theta, \varphi)$  depend mainly on the quantity  $H_c^*(j) = \langle H_c(j) \rangle / k$  and, to a minor extent, on the proportionality factors for  $\sigma_l$  and  $\sigma_c$ .  $H_c^*(j)$  represents the reduced mean critical field of the weak links, which depends on the intensity of the current density  $j$  and on the flux compression factor  $k$ . Thus, according to the present model, comparing the experimental data with the theoretical results allows the determination of  $H_c^*(j)$  as the main best-fit parameter, whose value is only little affected by the other two parameters  $\sigma_l$  and  $\sigma_c$ .  $H_c(j)$  can thus be taken as a quantity apt to characterize the “strength” of the weak-link ensemble and it is strongly dependent on the type of granular superconducting material. It has been observed that thermal treatments can produce strong changes in this quantity, leaving practically unaffected the superconducting properties of the grains, i.e., the critical temperature and the value of the magnetic field at

which the flux begins to penetrate into the grains.<sup>18</sup>

In conclusion, we have presented a simple model that is able to explain the anisotropy of the resistance shown by granular HTSC's in the presence of a magnetic field. The model can be applied if the intensity of the applied magnetic field is such that the bulk superconductivity is disrupted, but the grains remain in the superconducting state. This physical requirement is easily fulfilled in samples where the connections between grains is weak, as a result, for instance, of thermal treatments and annealing processes. In these conditions, we have shown that there is no need of assuming an intrinsic dependence of the intergrain resistivity on the angle between  $\mathbf{H}$  and  $\mathbf{j}$ , as instead the models based on the conventional theories of current-driven flux motion do. Incidentally, the motion of unpinned vortices is actually the main origin of the resistance in those materials where the links between grains are so strong that the flux can penetrate into the grains and even become unpinned well before the resistive transition of the weak links sets in.<sup>3</sup>

If the material is made up of weakly linked grains, instead, the local magnetic field and the local current density in a given weak link are *always* perpendicular to each other, provided that the flux penetration into the grains is negligible. In this case the proposed model, which describes the anisotropy of the resistivity as being due to the spatially anisotropic distribution of the resistive weak links seems more appropriate. Actually, the results of the model are in reasonable agreement with the experimental data obtained from resistance measurements in a YBCO granular specimen that satisfies the above-mentioned conditions. Good experimental evidence is also found for the inverse proportionality between the mean critical field of the weak links and the current density, which is the basic assumption over which the proposed model has been developed.

## ACKNOWLEDGMENTS

The authors wish to thank the late Professor P. Manca of the University of Cagliari for supplying the YBCO sample used for the reported measurements.

\*Electronic address: mazzetti@polito.it

<sup>1</sup>M. Tinkham and C. J. Lobb, *Solid State Phys.* **42**, 91 (1989).

<sup>2</sup>A. Barone and G. Paternò, *Physics and Applications of the Josephson Effect* (Wiley, New York, 1985).

<sup>3</sup>A. K. Pradhan, Z. X. Shi, M. Tokunaga, T. Tamegai, Y. Takano, K. Togano, H. Kito, and H. Ihara, *Phys. Rev. B* **64**, 212509 (2001).

<sup>4</sup>A. R. Jones, R. A. Doyle, F. J. Blunt, and A. M. Campbell, *Physica C* **196**, 63 (1992).

<sup>5</sup>B. A. Glowacki, M. Ciszek, S. Wu, and W. Y. Liang, *J. Supercond.* **11**, 1 (1998).

<sup>6</sup>M. M. Asim and S. K. Hasanain, *Solid State Commun.* **80**, 719 (1991).

<sup>7</sup>A. Kiliç, K. Kiliç, S. Senoussi, and K. Demir, *Physica C* **294**, 203 (1998).

<sup>8</sup>M. Chandran and P. Chaddah, *Supercond. Sci. Technol.* **8**, 774 (1995).

<sup>9</sup>D. López and F. de La Cruz, *Phys. Rev. B* **43**, 11 478 (1991).

<sup>10</sup>H. A. Blackstead, D. B. Pulling, P. J. McGinn, and C. A. Clough, *Physica C* **175**, 534 (1991).

<sup>11</sup>S. L. Ginzburg, V. P. Khavronin, and I. D. Luzyanin, *Supercond. Sci. Technol.* **11**, 255 (1998).

<sup>12</sup>J. Evetts and B. A. Glowacki, *Cryogenics* **28**, 641 (1988).

<sup>13</sup>J. Jackiewicz and J. Leszczynski, *Supercond. Sci. Technol.* **5**, S387 (1992).

<sup>14</sup>E. Altschuler, S. García, and J. Barroso, *Physica C* **177**, 61 (1991).

<sup>15</sup>W. F. Huang, K. J. Hung, and J. G. Shen, *Physica C* **208**, 7 (1993).

<sup>16</sup>P. G. de Gennes, *Superconductivity of Metals and Alloys* (W. A. Benjamin, New York, 1966), p. 27.

<sup>17</sup>See, for example, L. Cattaneo, M. Celasco, A. Masoero, P. Mazzetti, I. Puica, and A. Stepanescu, *Physica C* **267**, 127 (1996), and references therein.

<sup>18</sup>P. Mazzetti, A. Stepanescu, P. Tura, A. Masoero, and I. Puica, *Phys. Rev. B* **65**, 132512 (2002).